Melting Behavior of Bromobenzene within Carbon Nanotubes†

ARTICLE *in* JOURNAL OF CHEMICAL & ENGINEERING DATA · AUGUST 2010

Impact Factor: 2.04 · DOI: 10.1021/je1002576

2 AUTHORS:

Malgorzata Sliwinska-Bartkowiak
Adam Mickiewicz University
74 PUBLICATIONS **2,674** CITATIONS
SEE PROFILE

Monika Jazdzewska
Adam Mickiewicz University
8 PUBLICATIONS **69** CITATIONS
SEE PROFILE

Melting Behavior of Bromobenzene within Carbon Nanotubes†

Malgorzata Sliwinska-Bartkowiak* and Monika Jazdzewska

Institute of Physics, Adam Mickiewicz University, Umultowska 85, 61-614 Poznan, Poland

Keith E. Gubbins and Liangliang Huang

Department of Chemical and Biomolecular Engineering, North Carolina State University, Raleigh, North Carolina 27695-7905

We report experimental results on the melting behavior of a dipolar substance, bromobenzene, adsorbed in multiwalled carbon nanotubes (MWNTs) of (2.4, 4.0, and 10) nm inner diameter. Dielectric relaxation spectroscopy (DRS) and differential scanning calorimetry (DSC) methods have been used to show a solid−liquid transition of confined C_6H_5Br. The C_6H_5Br melting point in pores has been found to increase with decreasing pore diameter. This result is in qualitative agreement with that obtained in molecular simulation for CCl_4 in similar MWNTs, where the adsorbate−wall interactions are strong compared to the adsorbate−adsorbate interactions (see Jazdzewska et al., *Phys. Chem. Chem. Phys.* **2005**, *7*, 3884−3887).

Introduction

Recent studies for pores of simple geometry have shown a rich phase behavior associated with melting in confined systems.[1−15] The melting temperature may be lowered or raised relative to the bulk freezing temperature, depending on the nature of the adsorbate and the porous material. In addition, new surface-driven phases may intervene between the liquid and the solid phases in the pores. Contact layer phases of various kinds are often formed, in which the layer of adsorbed molecules adjacent to the pore wall has a different structure from that of the adsorbate molecules in the interior of the pore. These contact layer phases have been predicted theoretically and confirmed experimentally for several systems.[5,10] In addition, in some systems in which strong layering of the adsorbate occurs (e.g., activated carbon fibers), hexatic phases can occur; such phases have quasi-long-ranged orientational order, but positional disorder, and for quasi-two-dimensional systems occur over a temperature range between those for the crystal and liquid phases. These are clearly seen in molecular simulations, and recent experiments provide convincing evidence for these phases.[15] It has been shown that this apparently complex phase behavior results from a competition between the fluid−wall and fluid−fluid intermolecular interactions. For a given pore geometry and width, the phase diagrams for a wide range of adsorbates and porous solids can be classified in terms of a parameter α which is the ratio of the fluid−wall to fluid−fluid attractive interaction.[2,10,15] In this paper we report experimental studies of melting in multiwalled carbon nanotubes (MWNTs); experimental results from dielectric relaxation spectroscopy (DRS) and differential scanning calorimetry (DSC) are reported for C_6H_5Br in MWNTs of various diameters.

Methods

We report experimental studies of the melting transition for bromobenzene confined in opened multiwall carbon nanotubes of mean inner diameters of (2.4, 4.0 and 10) nm, produced and characterized by Nanocyl Co., Belgium. DSC and DRS were used to determine the melting temperature of confined C_6H_5Br. The MWNTs samples were heated to about 400 K and kept under vacuum (10^{-3} Tr) for a few days to remove air prior to and during the introduction of the liquids. The C_6H_5Br samples were reagent grade chemicals and were distilled twice under reduced pressure prior to their use in experiments. The conductivity of purified C_6H_5Br was of the order of $10^{-9}\ \Omega^{-1}\cdot m^{-1}$.

Differential Scanning Calorimetry. A Netzsch DSC204 Phoenix differential scanning calorimeter (DSC) was used to determine the melting temperatures of the confined bromobenzene by measuring the heat released in the melting of bromobenzene. Temperature scanning rates of (2 to 5) K min^{-1} were used in the experiments. The melting temperatures were determined from the position of the peaks of the heat flow signals during the warming process and were reproducible to within 0.5 K.

Dielectric Relaxation Spectroscopy. The melting of C_6H_5Br confined in MWNTs has also been investigated by DRS, as described elsewhere.[15] The dielectric constant is a natural choice of order parameter to study melting of dipolar liquids, because of the large change in the orientational polarizability between the solid and the liquid phases.[16] The complex electric permittivity, $\kappa = \kappa' + i\kappa''$, where $\kappa' = C/C_0$ is the real, and $\kappa'' = \tan(\delta)/\kappa'$ is the complex, part of the permittivity, was measured in the frequency interval (10^6 to 10) MHz at different temperatures using a Solartron 1260 impedance gain analyzer, with a parallel plate capacitor made of stainless steel. Here C is the electric capacitance, C_0 the capacitance in the absence of the dielectric medium, and δ the angle by which the current leads the voltage due to dielectric loss. To reduce the high conductivity of the sample, which was placed between the capacitor plates as a suspension of substance-filled MWNTs in pure liquids, the electrodes were covered with a thin layer of Teflon. The layer of Teflon does not change the profile of the capacity in function of frequency, but it has a constant influence on the capacity value relative to the capacitor without the Teflon layer (Figure 1). From the directly measured capacitance, C, and the tangent loss, $\tan(\delta)$, the values of κ' and κ'' were calculated for the known sample geometry. The temperature was stabilized using K30 Modingen external cryostat coupled with a N-180 ultracryostat. The temperature was controlled to an accuracy of 0.1 K using a platinum resistor Pt(100).

† Part of the "Sir John S. Rowlinson Festschrift".

* Corresponding author. E-mail: msb@amu.edu.pl.

10.1021/je1002576
Published on Web 08/25/2010

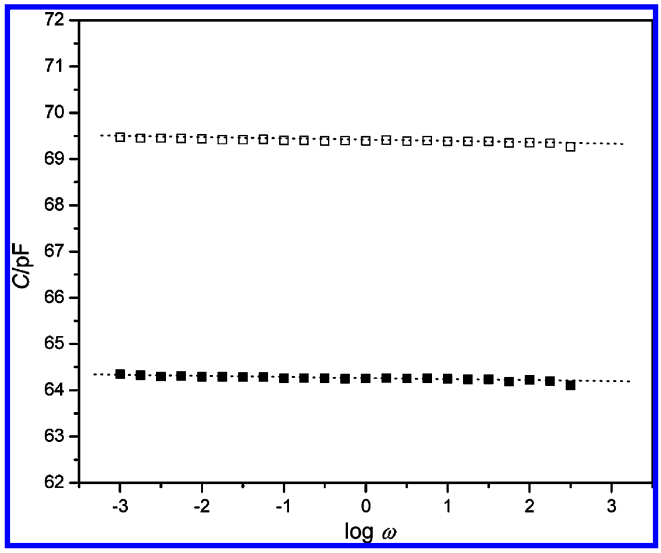

Figure 1. C vs log ω for: □, empty capacitor; ■, empty capacitor with a thin layer of Teflon.

For an isolated dipole rotating under an oscillating field in a viscous medium, the Debye dispersion relation is derived in terms of classical mechanics

$$\kappa^* = \kappa'_\infty + \frac{(\kappa'_s - \kappa'_\infty)}{(1 + i\omega\tau)} \quad (1)$$

where ω is the frequency of the potential applied and τ is the orientational relaxation time of a dipolar molecule. The subscript s refers to the static permittivity, that is, the permittivity in the low frequency limit, when the dipoles have enough time to be in phase with the applied field. The subscript ∞ refers to the high frequency limit of the permittivity and is a measure of the induced component of the permittivity. The dielectric relaxation time was calculated by fitting the dispersion spectrum of the complex permittivity near resonance to the Debye model of orientational relaxation.

Experimental Results

The melting temperature of C_6H_5Br confined in MWNTs with inner diameters of (2.4, 4.0, and 10) nm were determined using DSC and dielectric methods. Results of the measurements of C for bulk C_6H_5Br during the heating process as a function of T and at a frequency of 0.6 MHz are shown in Figure 2. There is a sharp increase in C at $T = 243$ K, the melting point of the pure substance, due to the contribution to the orientational polarization[11,12] in the liquid state from the permanent dipoles. In the frequency interval studied we could only detect the low frequency relaxation of C_6H_5Br.

Analysis of the Cole−Cole representation of the complex capacity for solid C_6H_5Br has shown that the relaxation observed should be approximated by a symmetric distribution of relaxation times described formally by the Cole−Cole eq 1. Examples of the experimental results and the fitted curves are given in Figure 3a,b and Figure 4a,b for the C_6H_5Br bulk solid phase at 209 K and for the C_6H_5Br liquid phase at 267 K. From the plot of κ' and κ'' versus log ω (Figure 3), the relaxation time can be calculated as the inverse of the frequency ω corresponding to a saddle point of the κ' plot or a maximum of the κ'' plot. An alternative graphical representation of the Debye dispersion equation is the Cole−Cole diagram in the complex κ^* plane (Figure 3b). Each relaxation mechanism is reflected as a semicircle in the Cole−Cole diagram. From the plot of κ'' versus κ', the value of τ is given as the inverse of the

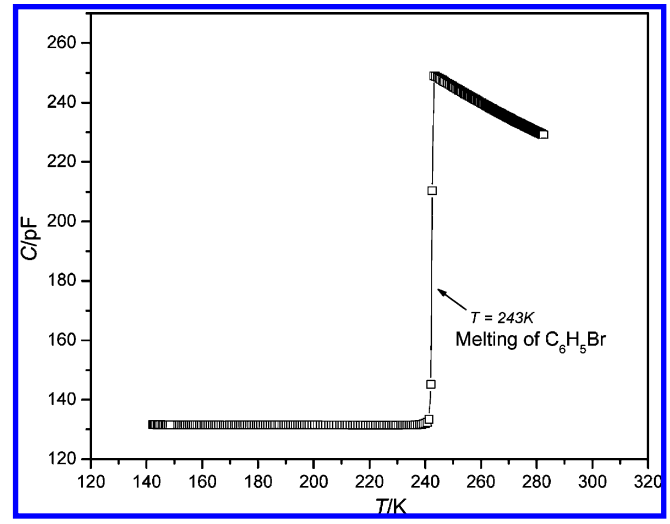

Figure 2. $C(T)$ for bromobenzene.

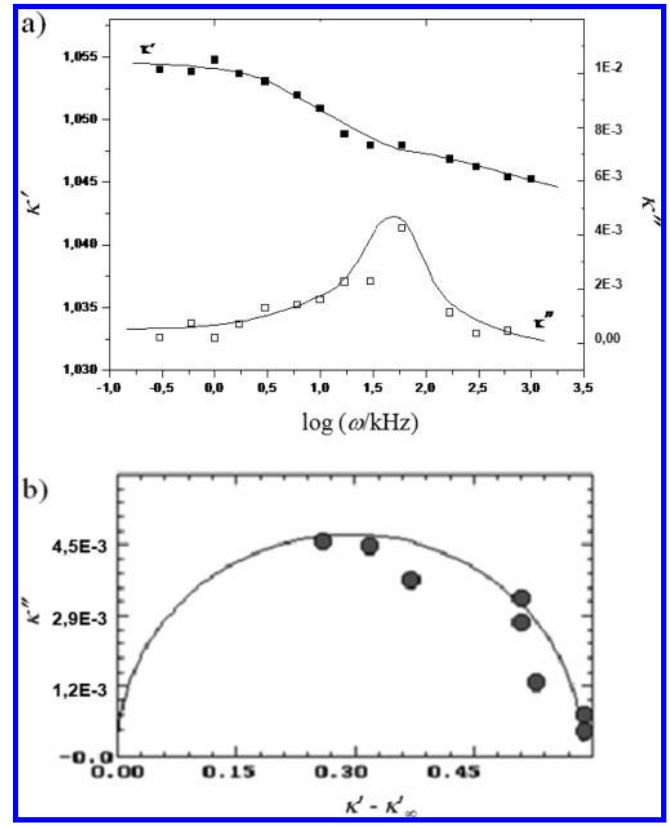

Figure 3. (a) Spectrum plot for C_6H_5Br at 209 K (the solid state); (b) representation of the spectrum plots in the form of a Cole−Cole diagram for C_6H_5Br at 209 K.

frequency at which κ'' goes through a maximum. Figure 5 presents the variation of the relaxation time with temperature for bulk C_6H_5Br obtained from fitting eq 1 to the dispersion spectrum. In the solid phase of C_6H_5Br (below 243 K), our measurements showed the solid state (the crystal form) to have a single relaxation time of the order of (10^{-5} to 10^{-6}) s in the temperature range from 200 K to about 243 K. At temperatures above the C_6H_5Br melting point of 243 K a drastic change of the value of the relaxation time is observed, related to the transition to the liquid phase. The corresponding Cole−Cole diagram is shown in Figure 4b. In the presence of dipolar constituents, one or more absorption regions are present, not all of them necessarily associated with the dipolar dispersion. At the lowest frequencies (especially about 1 kHz), a large κ'' value arises from the conductivity of the medium, and

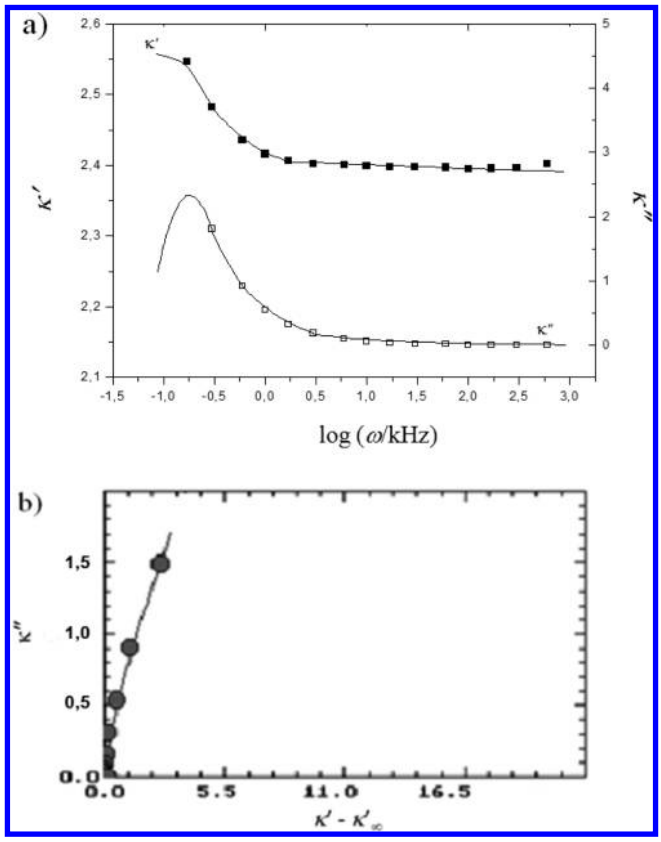

Figure 4. (a) Spectrum plot for C_6H_5Br at 267 K (the liquid state); (b) representation of the spectrum plots in the form of a Cole−Cole diagram for C_6H_5Br at 267 K.

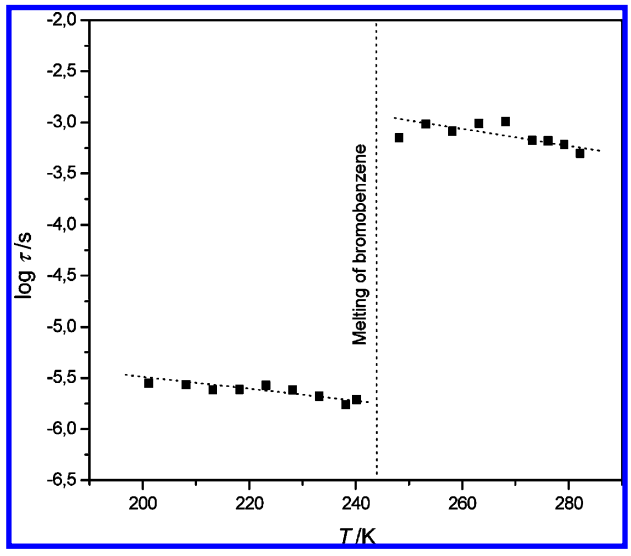

Figure 5. Dielectric relaxation time τ vs T for C_6H_5Br.

interfacial (Maxwell−Wagner) polarization is observed. For C_6H_5Br, a homogeneous medium whose conductivity is of the order of 10^{-9} $\Omega^{-1}\cdot m^{-1}$, the absorption region observed for the frequencies close to 1 kHz is related to the conductivity of the medium. The Joule heat arising from the conductivity contributes to a loss factor κ'' (conductance) so that the value at low frequency is: $\kappa''_{total} = \kappa''_{dielectric} + \kappa''_{conductance}$, and the system reveals the energy loss in processes other than dipolar relaxation.[17,18] In Figure 4b the component of the relaxation time of the order of 10^{-3} s characterizes the process of absorption related to the conductivity of the medium. This branch, strongly dependent on temperature, is characteristic of the liquid phase and is a good indicator of the appearance of the phase.

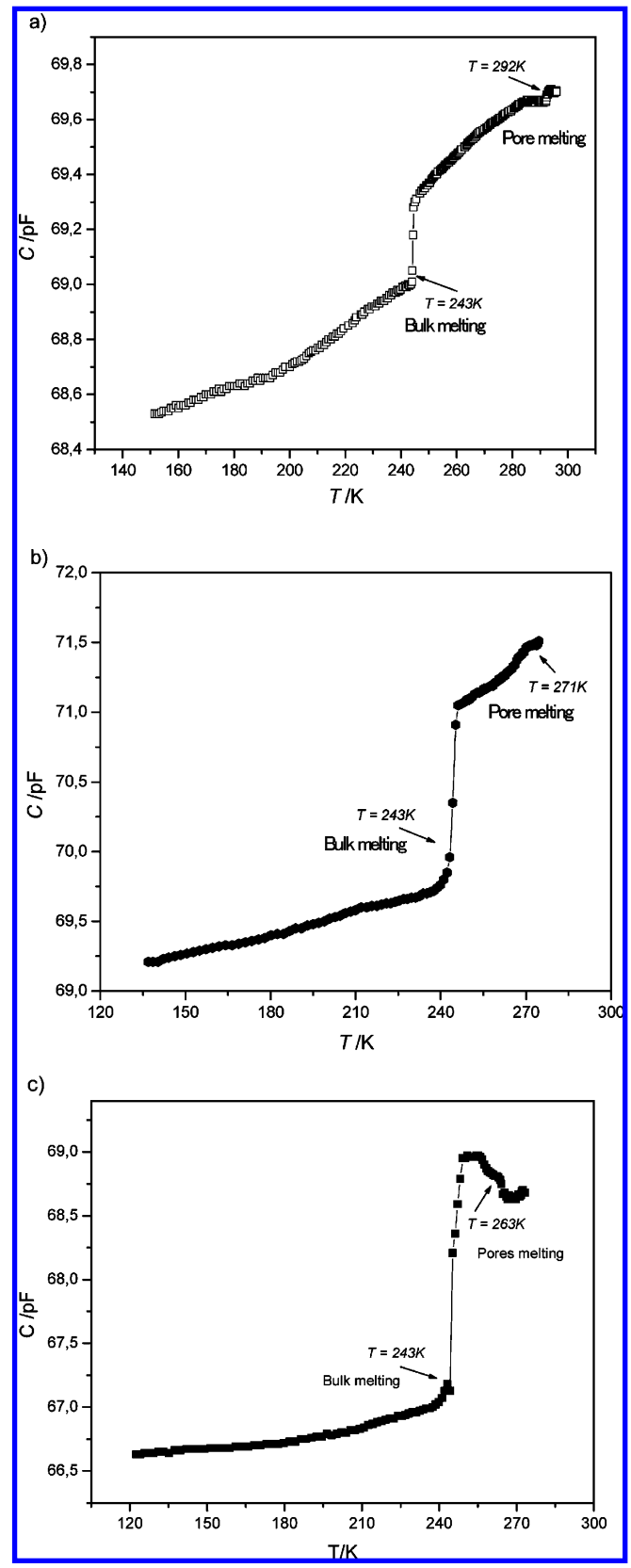

Figure 6. Electric capacity C vs temperature T for C_6H_5Br confined in MWNT: (a) 2.4 nm; (b) 4.0 nm; (c) 10 nm.

The melting temperatures of C_6H_5Br confined in MWNTs with inner diameters of (2.4, 4.0, and 10) nm were determined using DRS and DSC methods. In Figure 6 the capacity C as a function of temperature for C_6H_5Br confined in MWNTs of diameters (2.4, 4.0, and 10) nm is presented. Since the samples studied are a

suspension of C_6H_5Br-filled carbon nanotubes in pure C_6H_5Br, the signals contain both contributions of bulk and confined C_6H_5Br. In Figure 6a the feature observed at $T = 243$ K in the capacity C versus temperature plot was found at the same temperature for C_6H_5Br adsorbed on the pristine MWNTs. Since the latter are essentially closed, this discontinuity is associated with the melting point of bulk C_6H_5Br. By contrast, the increase in the $C(T)$ function observed at 292 K (Figure 6a) is attributed to melting in the pores. The shift of the melting temperature of C_6H_5Br bulk and in MWNT is: $\Delta T = T_{MWNT} - T_{bulk} = 49$ K. Figure 6b presents the function $C(T)$ for C_6H_5Br in MWNT of 4.0 nm diameter. The sharp increase in C at $T = 243$ K corresponds to bulk C_6H_5Br; the pore melting point is attributed to an increase in the $C(T)$ function at 271 K. For this system the shift of the melting temperature of bromobenzene in the MWNTs relative to that in the bulk is $\Delta T = 28$ K. In Figure 6c the $C(T)$ function for C_6H_5Br in MWNTs of diameter of 10.0 nm is presented. The increase in the capacity at $T = 243$ K corresponds to bulk melting temperature; the change in the $C(T)$ function observed at 264 K can be related to melting of confined C_6H_5Br. The shift of the melting temperature of C_6H_5Br in this case is $\Delta T = 21$ K, so the elevation of the melting temperature of C_6H_5Br in pores decreases with increasing diameter of the MWNT.

Similar results were obtained using the DSC method. The melting temperatures were determined from the position of the peaks of the heat flow signals on heating and were reproducible to within 0.5 K. An exemplary DSC scan corresponding to the melting of C_6H_5Br in MWNTs of 2.4 nm diameter is presented in Figure 7a. The large endothermic peak at 243 K corresponds to the melting of the bulk C_6H_5Br in which MWNTs are suspended in C_6H_5Br, so the pores are fully filled. In addition, a second peak at 293 K is observed, which can correspond to the melting of C_6H_5Br in MWNTs; the melting temperature of C_6H_5Br adsorbed in MWNTs is shifted toward higher temperatures by about 49 K relative to that of the bulk C_6H_5Br. Figure 7b presents a DSC scan for C_6H_5Br in MWNTs of 4.0 nm diameter. The large peak correspond to the melting of the bulk C_6H_5Br and the second peak at 271 K indicates the melting point of C_6H_5Br in the pores. The shift of the melting temperatures ΔT for C_6H_5Br is $\Delta T = 27$ K and is about 20 K lower than for C_6H_5Br in MWNTs of 2.4 nm diameter. In Figure 7c the DSC scan for C_6H_5Br in MWNTs of diameter of 10 nm is presented. The peak at 243 K indicates the melting of the bulk bromobenzene, and the smaller peak observed at 263 K corresponds to the melting of C_6H_5Br in the pores. The shift of melting temperature is $\Delta T = 20$ K.

Results of the analysis of the Cole−Cole representation of the complex capacity for C_6H_5Br placed in MWNTs of 4.0 nm diameter at various temperatures are shown in Figures 8 to 10. On the basis of the hitherto obtained results, it can be assumed that solid C_6H_5Br confined in MWNTs of 4.0 nm diameter melts at 271 K; below this temperature the system should contain solid C_6H_5Br in pores and liquid C_6H_5Br in the bulk. At temperatures lower than 243 K it should be present in the bulk crystal phase and also in the solid state in the pores. At temperatures higher than 271 K the bulk and confined C_6H_5Br are in the liquid phase. Figures 8 to 10 present the spectrum plot (κ', κ'' vs ω) for C_6H_5Br confined in MWNTs of 4.0 nm diameter at three different temperatures. The spectrum in Figure 8a for 222 K represents one relaxation mechanism, as indicated by the one inflection point in κ'' characterized by relaxation time of the order of 10^{-6} s. This value of relaxation time is typical of the bulk crystal phase. The corresponding Cole−Cole diagram is shown in Figure 8b. The spectrum for 261 K presented in Figure 9a represents two relaxation mechanisms corresponding to two semicircles in the Cole−Cole diagram (Figure 9b) and is characterized by the relaxation time of the order 10^{-6} s (similar to that for the bulk crystal phase at this temperature) and relaxation time of the order 10^{-2} s. The longer component of the relaxation is related to the Maxwell−Wagner−

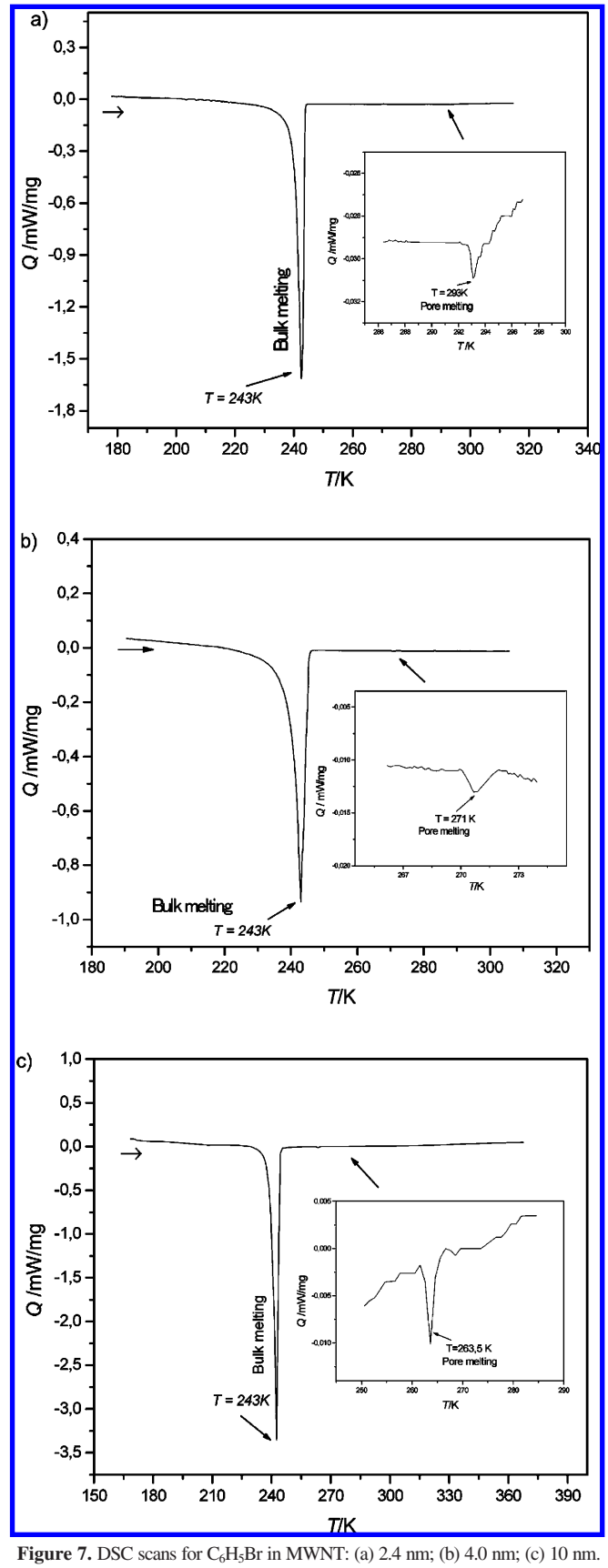

Figure 7. DSC scans for C_6H_5Br in MWNT: (a) 2.4 nm; (b) 4.0 nm; (c) 10 nm.

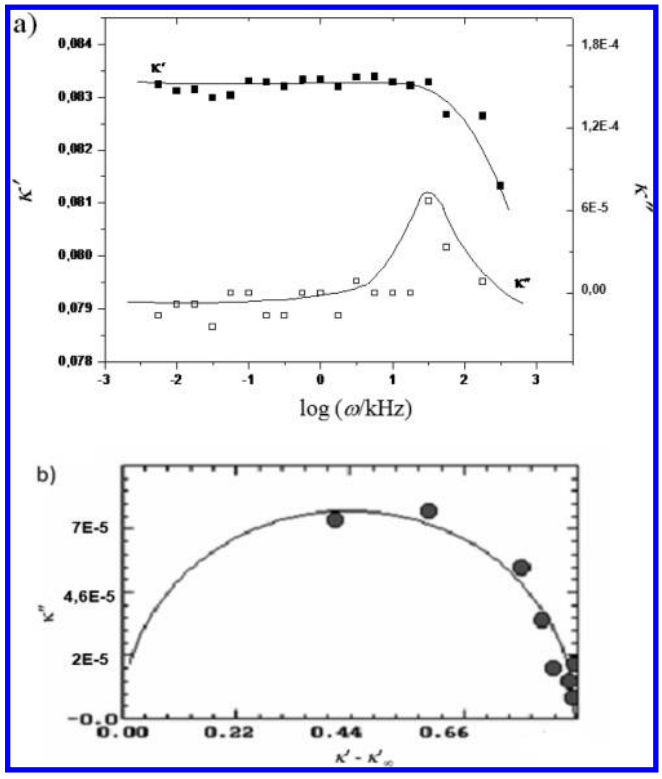

Figure 8. (a) Spectrum plot for C_6H_5Br in MWNTs of 4.0 nm diameter at 220 K; (b) representation of the spectrum plots in the form of a Cole−Cole diagram.

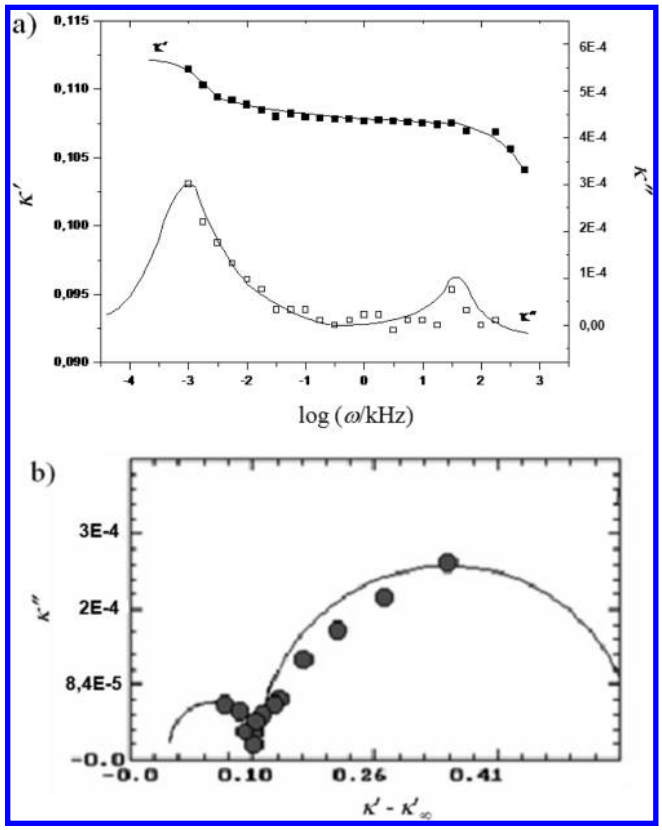

Figure 9. (a) Spectrum plot for C_6H_5Br in MWNTs of 4.0 nm diameter at 261 K; (b) representation of the spectrum plots in the form of a Cole−Cole diagram.

Sillars (MWS) polarization. For a heterogeneous system (when the MWNTs are suspended in the liquid), there occurs a relaxation mechanism related to the interfacial polarization, when a slightly

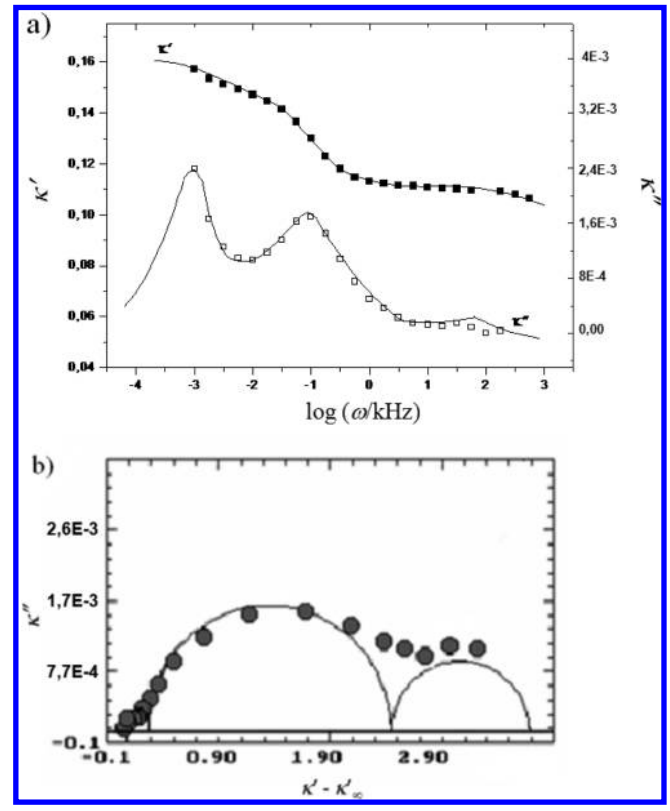

Figure 10. (a) Spectrum plot for C_6H_5Br in MWNTs of 4.0 nm diameter at 274 K; (b) representation of the spectrum plots in the form of a Cole−Cole diagram.

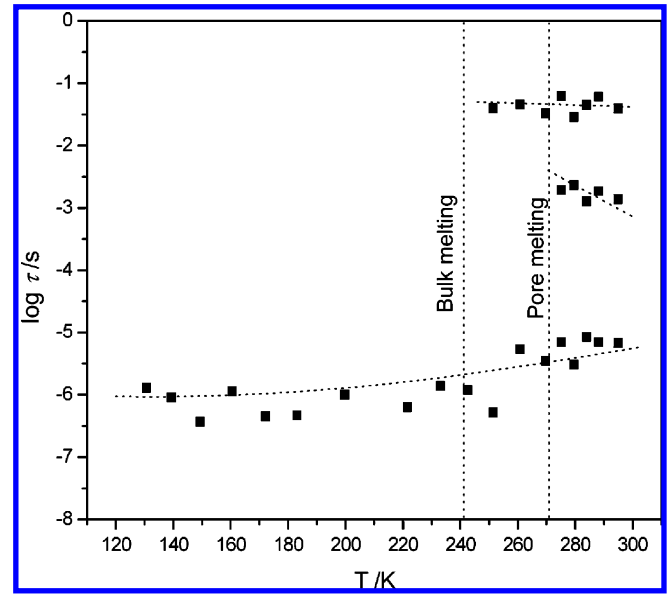

Figure 11. Dielectric relaxation time τ vs T for C_6H_5Br in MWNTs of diameter 4.0 nm.

conducting liquid is enclosed in a material of different conductivity. This effect, MWS polarization, is known to have a relaxation time of the order of (10^{-3} to 10^{-2}) s.[11] The spectrum plot at 280 K, presented at Figure 10, represents three relaxation mechanisms corresponding to three semicircles in the Cole−Cole diagram and characterized by a relaxation time of order 10^{-2} s (typical of MWS polarization) and a relaxation time of the order of 10^{-3} s (related with the conductivity of the liquid), and we can also distinguish a shorter component of relaxation time of the order of 10^{-5} s.

The behavior of the relaxation times as a function of temperature for C_6H_5Br in MWNTs of diameter of 4.0 nm is

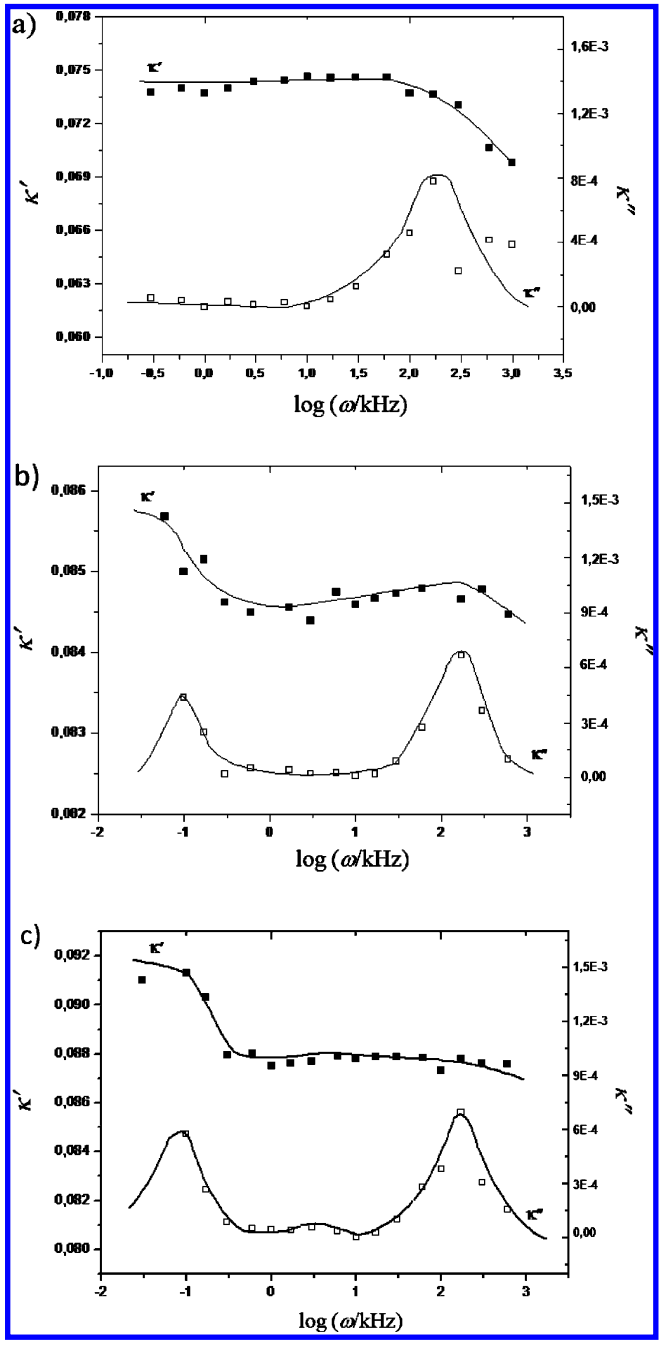

Figure 12. Spectrum plot for C_6H_5Br in MWNTs of diameter 2.4 nm: (a) at 218 K; (b) at 268 K; (c) at 293 K.

depicted in Figure 11. For temperatures higher than 271 K (melting point inside the pores) there are three different kinds of relaxation. The larger component of the relaxation time of the order of 10^{-2} s appears in the system above the bulk melting temperature and can be related with interfacial MWS polarization. The branch of relaxation time of the order of 10^{-3} s, which can be observed above the pore melting point, more dependent on temperature, can be related to the conductivity of C_6H_5Br in the pores and testifies to the presence of the liquid phase in pores. The shorter component of the relaxation time is of the order of 10^{-5} s and can characterize the Debye relaxation of the liquid C_6H_5Br in the pores. Molecular simulation results for CCl_4 in MWNTs of (2.8 and 4) nm diameter show that before the melting temperature all adsorbate regions behave as dense, liquid-like fluids with short-range positional and bond orientational order,[1] so the branch of relaxation time of the order of

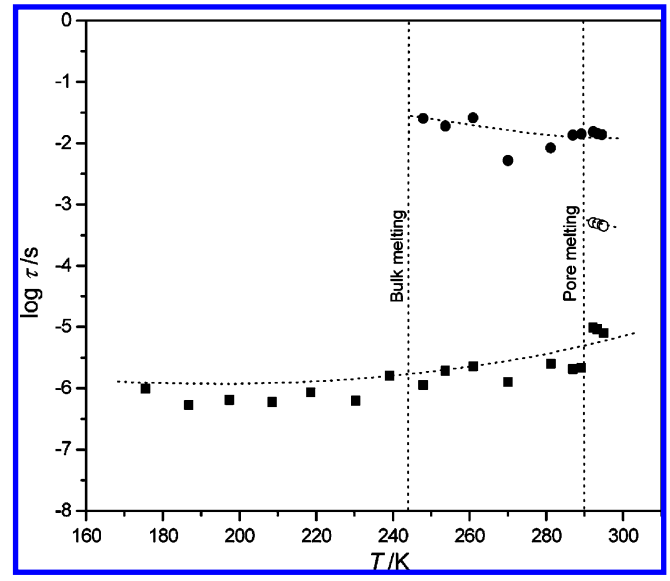

Figure 13. Dielectric relaxation time τ vs T for C_6H_5Br in MWNTs of diameter 2.4 nm.

10^{-5} s, which is much lower than for the bulk liquid, can be related to the adsorbate. In the temperature region (271 to 243) K, we still observe the branch of relaxation time related to MWS polarization and a branch with relaxation time values similar for the crystal C_6H_5Br phase. The simulation results for CCl_4 in MWNTs of diameter (2.8 and 4) nm show that below the pore melting point CCl_4 has an intermediate morphology between the crystal and the liquid,[1] so the branch of the relaxation time of the order of 10^{-6} s can reflect a similar phase of confined C_6H_5Br. Such results are confirmed by a very small DSC signal observed at the pore melting point. In the temperature range below 243 K one branch of the relaxation time is observed which can be related to the crystal phase of the bulk and confined C_6H_5Br.

In Figure 12 a spectrum plot for C_6H_5Br confined in MWNTs of diameter of 2.4 nm is presented. In the solid phase (below 243 K) the spectrum represents one relaxation mechanism with relaxation time of the order of 10^{-6} s (Figure 12a). The spectrum in Figure 12b for 268 K shows two relaxation mechanisms which correspond to relaxation times of the order 10^{-6} s and 10^{-2} s. In Figure 12c the spectrum for 293 K presents three relaxation mechanisms characterized by relaxation times of the order of 10^{-5} s, 10^{-3} s, and 10^{-2} s. Distribution of the relaxation times for C_6H_5Br confined in MWNTs of diameter of 2.4 nm is presented in Figure 13. For temperatures higher than the pore melting point, again three branches of the relaxation time are depicted; below the pore melting point the branch of about 10^{-6} s, close to the bulk crystal phase, exists, which can be related to an intermediate morphology between the crystal and a liquid. At lower temperatures, below 243 K, we observe only one branch of relaxation time, typical of the crystal phase. The branch corresponding to confined C_6H_5Br is too difficult to separate experimentally at this temperature region.

In Figure 14 the shifts of melting temperature of bromobenzene in MWNTs of various diameters relatively to the bromobenzene bulk ΔT are presented. The elevation of the melting temperature of C_6H_5Br in pores decreases with increasing diameter of the MWNTs. This result is in qualitative agreement with that obtained in molecular simulation for CCl_4 in similar MWNTs, where the adsorbate−wall interactions are strong compared to the adsorbate−adsorbate interactions.[1]

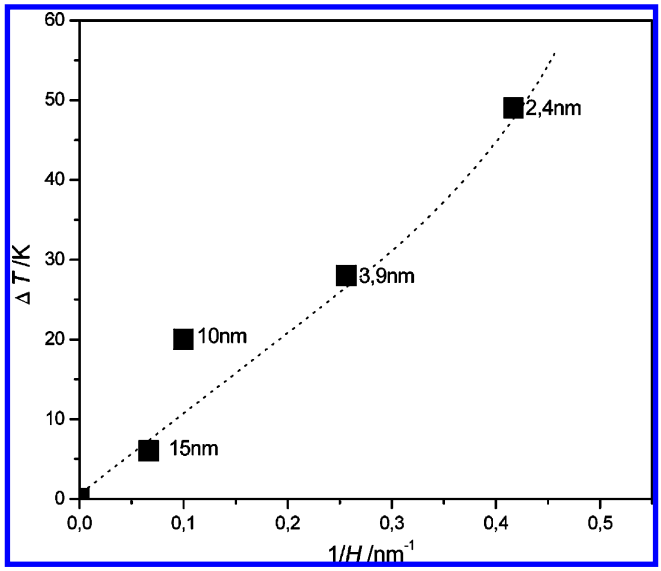

Figure 14. $\Delta T(1/H)$ for C_6H_5Br in MWNTs of diameter: 2.4 nm; 4.0 nm; 10 nm; and 15 nm.

Conclusions

We have presented DRS measurements of the melting behavior of C_6H_5Br within open-tip MWNTs with three different pore diameters of (10, 4.0, and 2.4) nm. In each cases, we have observed one transition corresponding to melting of the confined adsorbate, at temperatures well above the bulk melting point of C_6H_5Br ($T_m = 263$ K for $D = 10.0$ nm, $T_m = 271$ K for $D = 4.0$ nm, and $T_m = 292$ K for $D = 2.4$ nm). Simulation and experimental studies have shown that an elevation in the melting point is observed for systems where the adsorbate−wall interactions are strong compared to the adsorbate−adsorbate interactions.[1,3−10,14] MWNTs are representative of materials with strongly attractive cylindrical pores. This effect of the pore size has been observed in previous studies[1−16] of strongly attractive pores with cylindrical geometry and has been explained as follows: the adsorbate−wall attractive interactions dominate the phase behavior at the smaller pore diameters, leading to larger increases in the solidification temperatures of the molecular layers close to the walls.

Literature Cited

(1) Jazdzewska, M.; Hung, F. R.; Gubbins, K. E.; Sliwinska-Bartkowiaka, M. An Experimental Study of Melting of CCl_4 in Carbon Nanotubes. *Phys. Chem. Chem. Phys.* **2005**, *7*, 3884–3887.
(2) Gelb, L. D.; Gubbins, K. E.; Radhakrishnan, R.; Sliwinska-Bartkowiak, M. Phase Separation in Confined Systems. *Rep. Prog. Phys.* **1999**, *62*, 1573–1659.
(3) Miyahara, M.; Gubbins, K. E. Freezing/Melting Phenomena for Lennard-Jones Methane in Slit Pores: a Monte Carlo Study. *J. Chem. Phys.* **1997**, *106*, 2865–2880.
(4) Radhakrishnan, R.; Gubbins, K. E. Free Energy Studies of Freezing in Slit Pores: An Order-Parameter Approach Using Monte Carlo Simulation. *Mol. Phys.* **1999**, *96*, 1249–1267.
(5) Sliwinska-Bartkowiak, M.; Gras, J.; Sikorski, R.; Radhakrishnan, R.; Gelb, L. D.; Gubbins, K. E. Phase Transitions in Pores: Experimental and Simulation Studies of Melting and Freezing. *Langmuir* **1999**, *15*, 6060–6069.
(6) Dominguez, H.; Allen, M. P.; Evans, R. Monte Carlo Studies of the Freezing and Condensation Transitions of Confined Fluids. *Mol. Phys.* **1998**, *96*, 209–229.
(7) Kaneko, K.; Watanabe, A.; Iiyama, T.; Radhakrishnan, R.; Gubbins, K. E. A Remarkable Elevation of Freezing Temperature of CCl_4 in Graphitic Micropores. *J. Phys. Chem. B* **1999**, *103*, 7061–7063.
(8) Watanabe, A.; Kaneko, K. Melting Temperature Elevation of Benzene Confined in Graphitic Micropore. *Chem. Phys. Lett.* **1999**, *305*, 71–74.
(9) Radhakrishnan, R.; Gubbins, K. E.; Watanabe, A.; Kaneko, K. Freezing of Simple Fluids in Microporous Activated Carbon Fibers: Comparison of Simulation and Experiment. *J. Chem. Phys.* **1999**, *111*, 9058–9067.
(10) Radhakrishnan, R.; Gubbins, K. E.; Sliwinska-Bartkowiak, M. Effect of the Fluid-Wall Interaction on Freezing of Confined Fluids: Towards the Development of a Global Phase Diagram. *J. Chem. Phys.* **2000**, *112*, 11048–11057.
(11) Sliwinska-Bartkowiak, M.; Dudziak, G.; Sikorski, R.; Gras, R.; Radhakrishnan, R.; Gubbins, K. E. Melting/Freezing Behavior of a Fluid Confined in Porous Glasses and MCM-41: Dielectric Spectroscopy and Molecular Simulation. *J. Chem. Phys.* **2001**, *114*, 950–962.
(12) Sliwinska-Bartkowiak, M.; Dudziak, G.; Sikorski, R.; Gras, R.; Gubbins, K. E.; Radhakrishnan, R. Dielectric Studies of Freezing Behavior in Porous Materials: Water and Methanol in Activated Carbon Fibers. *Phys. Chem. Chem. Phys.* **2001**, *3*, 1179–1184.
(13) Sliwinska-Bartkowiak, M.; Radhakrishnan, R.; Gubbins, K. E. Effect of Confinement on Melting in Slit-Shaped Pores: Experimental and Simulation Study of Aniline in Activated Carbon Fibers. *Mol. Simul.* **2001**, *27*, 323–3337.
(14) Alba-Simionesco, C.; Coasne, B.; Dosseh, G.; Dudziak, G.; Gubbins, K. E.; Radhakrishnan, R.; Śliwinska-Bartkowiak, M. Effects of Confinement on Freezing and Melting. *J. Phys.: Condens. Matter* **2006**, *18*, R15–R68.
(15) Radhakrishnan, R.; Gubbins, K. E.; Sliwinska-Bartkowiak, M. Global Phase Diagrams for Freezing in Porous Media. *J. Chem. Phys.* **2002**, *116*, 1147–1155.
(16) Sliwinska-Bartkowiak, M.; Jazdzewska, M.; Huang, L. L.; Gubbins, K. E. Melting Behavior of Water in Cylindrical Pores: Carbon Nanotubes and silica Glasses. *Phys. Chem. Chem. Phys.* **2008**, *3*, 1179–1184.
(17) Chelkowski, A. *Dielectric Physics*; Elsevier: North-Holland, 1990.
(18) Szurkowski, B.; Hilczer, T.; Sliwinska-Bartkowiak, M. Temperature Dependence of the Permittivity of *o*-Nitroanisole−Benzene and *o*-Nitroanisole−Carbon Tetrachloride Mixtures in the Vicinity of its Melting Point. *Ber. Bunsen-Ges.* **1993**, *97*, 731.

Received for review March 18, 2010. Accepted August 13, 2010. This work was supported by grant from Polish Ministry of Science and High Education (Grant MNiSW No. N N202 070333) and from the U.S. National Science Foundation (Grant No. CBET-0932656).

JE1002576